

# The effect of stellar activity on the spectroscopic stellar parameters of the young solar twin HIP 36515

Jhon Yana Galarza,<sup>1</sup>★ Jorge Meléndez,<sup>1</sup> Diego Lorenzo-Oliveira,<sup>1</sup> Adriana Valio,<sup>2</sup> Henrique Reggiani,<sup>1</sup> Marília Carlos,<sup>1</sup> Geisa Ponte,<sup>2,3</sup> Lorenzo Spina,<sup>4</sup> Raphaëlle D. Haywood<sup>5</sup>† and Davide Gandolfi<sup>6</sup>

<sup>1</sup>Universidade de São Paulo, Departamento de Astronomia do IAG/USP, Rua do Matão 1226, Cidade Universitária, 05508-900 São Paulo, SP, Brazil

<sup>2</sup>CRAAM, Mackenzie Presbyterian University, Rua da Consolação, 896, São Paulo, Brazil,

<sup>3</sup>Universidade Federal do Rio de Janeiro, Observatório do Valongo, Ladeira do Pedro Antonio 43, CEP: 20080-090 Rio de Janeiro, RJ, Brazil,

<sup>4</sup>Monash Centre for Astrophysics, School of Physics and Astronomy, Monash University, VIC 3800, Australia,

<sup>5</sup>Harvard-Smithsonian Center for Astrophysics, 60 Garden Street, Cambridge, MA 02138, USA,

<sup>6</sup>Dipartimento di Fisica, Università degli Studi di Torino, via Pietro Giuria 1, I-10125, Torino, Italy

Accepted —. Received —; in original form —

## ABSTRACT

Spectroscopic equilibrium allows us to obtain precise stellar parameters in Sun-like stars. It relies on the assumption of the iron excitation and ionization equilibrium. However, several works suggest that magnetic activity may affect chemical abundances of young active stars, calling into question the validity of this widely-used method. We have tested for the first time variations in stellar parameters and chemical abundances for the young solar twin HIP 36515 ( $\sim 0.4$  Gyr), along its activity cycle. This star has stellar parameters very well established in the literature and we estimated its activity cycle in  $\sim 6$  years. Using HARPS spectra with high resolving power (115 000) and signal-to-noise ratio ( $\sim 270$ ), the stellar parameters of six different epochs in the cycle were estimated. We found that the stellar activity is strongly correlated with the effective temperature, metallicity, and microturbulence velocity. The possibility of changes in the Li I 6707.8 Å line due to flares and star spots was also investigated. Although the core of the line profile shows some variations with the stellar cycle, it is compensated by changes in the effective temperature, resulting in a non variation of the Li abundance.

**Key words:** stars: solar-type – stars: abundances – stars: activity – stars: atmospheres – stars: fundamental parameters – techniques: spectroscopic

## 1 INTRODUCTION

Precise stellar parameters (effective temperature  $T_{\text{eff}}$ , metallicity  $[\text{Fe}/\text{H}]$ , surface gravity  $\log g$  and microturbulence velocity  $v_t$ ) are not only important for the characterization of stars themselves and to determine precise chemical abundances, but they are also key for characterizing exoplanets, as the planetary radius or planetary mass depends on the adopted properties of its host star. A common method to determine stellar parameters is through the spectroscopic equilibrium, which is performed by imposing the excitation and ionization balance, and evaluating the lack of dependence of iron abundance with reduced equivalent width. However, other techniques (e.g., via color-temperature calibration and asteroseismology) could be also employed to calculate  $T_{\text{eff}}$  (Casagrande et al. 2010) and  $\log g$  (Meléndez et al. 2006; Hekker et al. 2013; Campante et al. 2014). In spite of relatively good agreement between these methods, the

results could be quite different for young stars with ages of  $\sim 1$  Gyr (see Figs. 13 and 15 of Ramírez et al. 2014), and the problem may be even worse for younger and more active stars. Observational evidence of oxygen abundance variations (up to  $\sim 1$  dex) with  $T_{\text{eff}}$  in the Hyades cluster ( $\sim 0.6$  Gyr) were reported by Schuler et al. (2006), perhaps due to an overexcitation effect caused by active regions. Spina et al. (2014) showed that microturbulence of pre-main sequence stars are greater than those of main-sequence stars, and it could be related to the active chromospheres of young stars (Steenbock & Holweger 1981), which also have considerable impact on their abundance determination (Spina et al. 2017).

On the other hand, theoretical studies have demonstrated that magnetic fields could affect the stellar spectra in two ways: through forces on the stellar plasma that change the thermodynamical structure of the atmosphere (indirect effects) and through magnetic Zeeman broadening of the spectral lines (direct effects). Thus, the stellar parameters of young magnetically-active stars could not be as precise as we thought, due to the lack of inclusion of magnetic fields in classical one-dimensional model atmospheres (Castelli & Kurucz

★ E-mail: ramstojh@usp.br

† NASA Sagan Fellow

2003; Gustafsson et al. 2008). The problems described above could be exacerbated for Sun-like stars younger than about 200 Myr, due to the much higher magnetic field strength in those stars (Rosén et al. 2016).

Seminal theoretical studies have investigated the impact of magnetic fields on spectral line formation using 1D and 3D model atmospheres (Borrero 2008; Fabbian et al. 2010, 2012; Moore et al. 2015; Shchukina & Trujillo Bueno 2015; Shchukina et al. 2016). These authors found that several iron lines are sensitive to the aforementioned effects, resulting in variations of  $\sim 0.1$  dex in abundance. Besides, the impact of these effects on the abundance determinations could be reduced when the direct and indirect effects act in opposite ways. They also found that other elements such as C, O and Si are affected by magnetic fields, varying their abundance by about  $\sim 0.02$  dex. Furthermore, Flores et al. (2016) showed observational evidence of modulations ( $\sim 2$  mÅ) of the equivalent widths (hereafter  $EW$ ) of Fe II lines with the chromospheric cycle of the solar twin HIP 45184 (with  $\sim 5.1$  yr activity cycle and  $\langle S \rangle = 0.173$ ). However, Flores et al. (2018) were not able to find the similar modulations in HD 38858 ( $\sim 10.8$  yr activity cycle). Precise spectroscopic measurements in the Sun over more than three decades (Livingston et al. 2007), show small but measurable variations in some spectral lines (including some strong Fe I lines), but their dependence on the solar activity cycle is not well-established yet. The above studies question the validity of the spectroscopic equilibrium method for determining stellar parameters in young stars.

Lithium is an important element that has been used to study potential trends with stellar parameters, chromospheric activity, age and exoplanets (e.g., Do Nascimento et al. 2009; Ghezzi et al. 2010; Carlos et al. 2016). Enhancement of the neutral Li I at 6707.8 Å in the presence of sunspots was reported by Giampapa (1984). Other studies (e.g., Pallavicini et al. 1992; Fekel 1996; Barrado y Navascués et al. 1997) also found variation of Li  $EW$ s with stellar activity in chromospheric active binaries, pre-main-sequence stars and late-type dwarfs in very young clusters. Such enhancements were also observed even in flares of chromospheric active binary stars (Montes & Ramsey 1998). However, despite these large numbers of studies, the nature of the yield of Li I in starspots and flares is still inconclusive. The aim of this study is, therefore, to investigate for the first time, the influence of magnetic fields along the activity cycle on the stellar parameters and Li abundance of the young solar twin HIP 36515.

## 2 SPECTROSCOPIC OBSERVATIONS AND DATA REDUCTION

The spectra of the Sun (reflected light from the Vesta asteroid) and HIP 36515 were taken with the HARPS spectrograph at La Silla Observatory (3.6 m telescope) between 2014 to 2019, under the ESO (European Southern Observatory) programs: 192.C-0224(G), 192.C-0224(B), 192.C-0224(C), 0100.D-0444(A), 0101.C-0275(R) and 0103.D-0445. Each spectrum was automatically reduced by the HARPS data reduction software. The spectra have high resolving power  $R = \lambda/\Delta\lambda = 115\,000$  and cover a spectral range 3782–6913 Å. The red and blue part of the spectra were carefully normalized using the continuum task in IRAF, and then combined in order to obtain the highest possible SNR.

## 3 DATA ANALYSIS

### 3.1 Stellar Activity Cycle

The stellar and fundamental parameters ( $T_{\text{eff}}$ , [Fe/H],  $\log g$ , age, mass, and radius) of HIP 36515 were estimated with extremely high precision by Spina et al. (2018). This young active star ( $\sim 0.4$  Gyr) is an excellent candidate to explore the effects of magnetic fields on abundance determinations. The HARPS- $S$  index (hereafter  $S_{\text{HK}}$ ) was estimated measuring the chromospheric emission in the cores of the Ca II H and K lines ( $\langle S_{\text{HK}} \rangle = 0.3270 \pm 0.0226$ ), following the prescriptions presented in Lorenzo-Oliveira et al. (2018). In panel (a) of Fig. 1 is shown the activity cycle of HIP 36515 binned in 90 days. Inspecting our activity time-series, we estimated the  $S_{\text{HK}}$  amplitude variations induced by stellar rotation ( $\sigma_{S_{\text{HK}},\text{Prot}} = 0.0046$  and  $P_{\text{rot}} = 4.6 \pm 1.2$  days; Lorenzo-Oliveira et al. 2019). We propagated the activity variations within each night of observations ( $\sigma_{S_{\text{HK}},\text{night}} = 0.0007$ ) with the errors caused by rotational modulation weighted by the number of observing nights within each bin of 90 days ( $N_{\text{nights}}$ ):  $\sigma_{S_{\text{HK}},\text{bin}} \equiv \left( (\sigma_{S_{\text{HK}},\text{Prot}}^2)/N_{\text{nights}} + \sigma_{S_{\text{HK}},\text{night}}^2 \right)^{1/2}$ . The cycle period ( $P_{\text{cycle}}$ ) is estimated through Gaussian process (GP) fitting to account the quasi-periodic trends of stellar activity, represented in this case by  $S_{\text{HK}}$ . To do so, we choose an appropriate kernel function that combines white noise term ( $\sigma^2 \delta_{i,j}$ ) and exponential sine squared kernel which encapsulates important variables related to periodicity ( $f \equiv 1/P_{\text{cycle}}$ ), amplitude ( $\mathcal{A}$ ), and the harmonic nature ( $\Gamma$ ) of the time series. The adopted kernel function  $k(t_i, t_j)$  relates the covariance between two different epochs  $t_i$  and  $t_j$ :  $k(t_i, t_j) \equiv \mathcal{A} \exp \left( -\Gamma \sin^2 \left[ \pi f |t_i - t_j| \right] \right) + \sigma^2 \delta_{i,j}$ . All GP hyperparameters (GPH) are determined simultaneously using Markov chain Monte Carlo method (MCMC) optimization (Rasmussen & Williams 2006; Ambikasaran et al. 2015) resulting in the following median and 16% confidence interval values of  $0.043^{+0.021}_{-0.032}$ ,  $6.2^{+4.3}_{-0.4}$  years, and  $0.032^{+0.017}_{-0.012}$ , for  $\Gamma$ ,  $P_{\text{cycle}}$ , and  $\mathcal{A}_{S_{\text{HK}}}$ , respectively. These GPH compose the trained activity kernel which will help us to predict the spectroscopic activity induced effects by fixing the periodic GPH ( $\Gamma$  and  $P_{\text{cycle}}$ ) and leaving only  $\mathcal{A}_{\text{variable}}$  to scale according to the spectroscopic variable of interest (e.g.  $EW$ ,  $T_{\text{eff}}$ , [Fe/H], Li, and so on).

### 3.2 Equivalent Widths ( $EW$ s)

If magnetic fields change the shape of spectral lines, this will be reflected on their abundance determination. As discussed above, iron abundance variations ( $\sim 0.014$  dex) were only predicted in solar simulation spectra under extreme magnetic fields (80–200 G). To detect potential variation of spectral lines in HIP 36515, we selected strategically six bins from the activity cycle (see panel (b) of Fig. 1). Several spectra were combined in these bins in order to obtain a SNR  $\sim 270$ . The  $EW$  of iron lines (e.g., Meléndez et al. 2014) were measured along these epochs using the `splot` task in IRAF, fitting the line profiles with Gaussians. The mean uncertainty of the  $EW$  in each epoch is  $\sim 0.7$  mÅ. Pseudo-continuum regions were obtained following Bedell et al. (2014) in a window of 6 Å. The analysis is based on the line-by-line equivalent width technique (e.g. Meléndez et al. 2009; Yana Galarza et al. 2016; Spina et al. 2018).

The optical depth ( $\tau_\lambda$ ) of the iron lines are estimated by the radiative transfer code MOOG (Sneden 1973), as the depth at the corresponding wavelength and atmospheric layer, using the contribution function given by Edmonds (1969). Fig. 2 shows the difference in  $EW$ s of the iron lines between the maximum and the

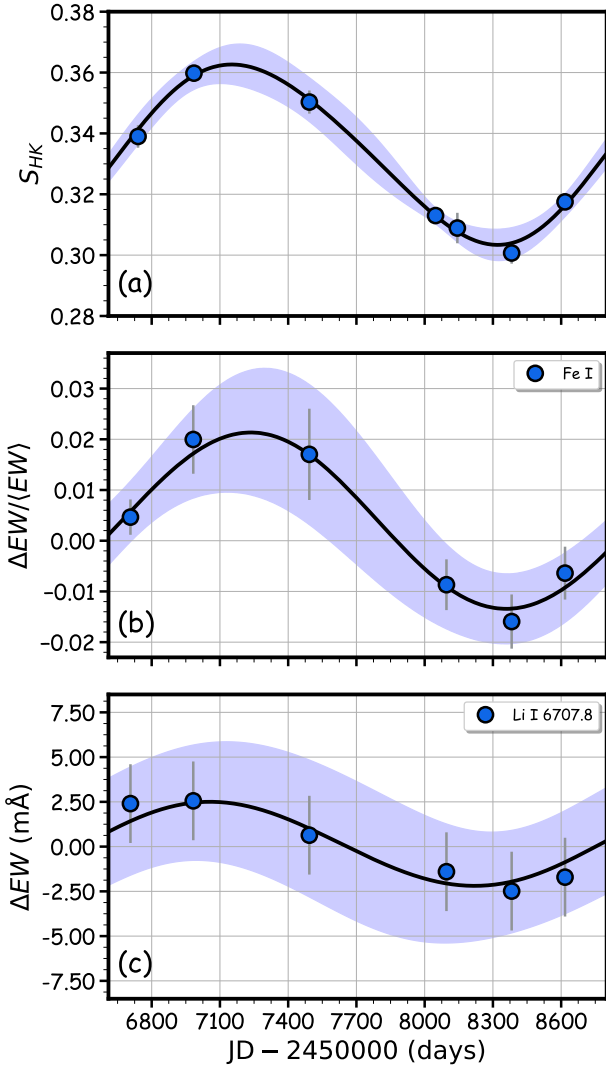


**Figure 1.** Panel (a): Activity cycle fit of HIP 36515 using Gaussian process (black line). Circles represent the  $S_{\text{HK}}$  values estimated in 7 epochs from 2014 to 2019. Panel (b): Relative changes of EWs of our sensitive Fe I lines (Table 1) along the stellar activity cycle. The black line in panel (b) and (c) represent the predicted changes generated by the activity kernel anchored on  $S_{\text{HK}}$  index. The shaded regions in all panels are the  $2\sigma$  activity variability prediction band. The standard deviation of the residuals computed from the measured and the GP activity induced spectroscopic predictions are 0.0019 and 0.6 mÅ for panel (b) and (c), respectively.

minimum of the stellar cycle (hereafter  $\Delta\text{EW}$ ) versus the mean line-center optical depth formation ( $\log_{10}(\tau_{\lambda})$ ). As in Shchukina & Trujillo Bueno (2015), we separated the iron lines by EWs and landé g-factor ( $g_L$ ) in four groups. The first two groups have  $\text{EW} < 40$  mÅ and are represented by stars ( $g_L \leq 1.5$ ) and squares ( $g_L \geq 1.5$ ) in both panels of Fig. 2. These lines are formed in regions close to the bottom photosphere ( $\log_{10}(\tau_{\lambda}) > -1$ ), and are into the shaded regions of Fig. 2, which represent the  $1.5\sigma$  of the mean uncertainty of the EWs, and do not produce relevant impact on the stellar parameter determinations (only 6 K in  $T_{\text{eff}}$ , 0.01 dex in  $\log g$ , 0.002 dex in  $[\text{Fe}/\text{H}]$ , and  $0.02 \text{ km s}^{-1}$  in  $v_t$ ; these values were estimated removing all  $\Delta\text{EW} > 1.0$  mÅ). The last two sets contain strong and

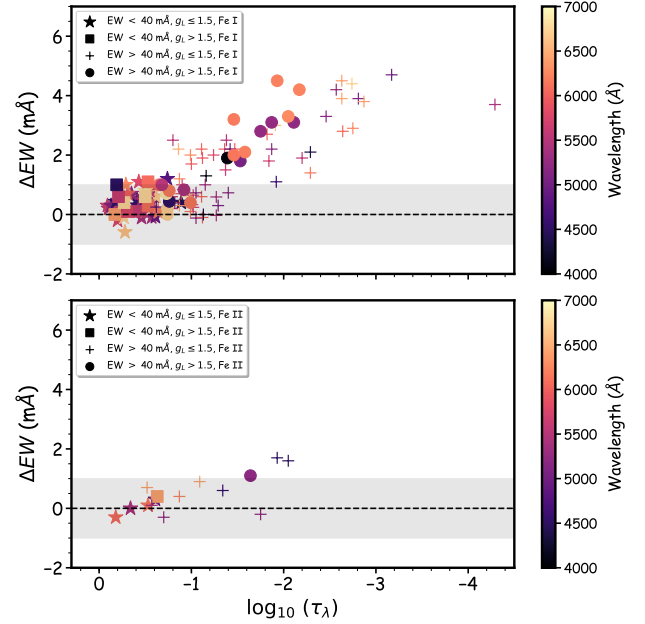


**Figure 2.** Differential  $\Delta\text{EW}$ s of Fe I (upper panel) and Fe II (bottom panel) lines versus their optical depths of formation  $\log_{10}(\tau_{\lambda})$ . The Fe I and Fe II are divided in four sets, and are colored by their wavelength. Iron lines into the shaded regions are not affected by stellar activity.

moderate iron lines ( $40 \text{ mÅ} < \text{EW} < 180 \text{ mÅ}$ ) and are represented by crosses ( $g_L \leq 1.5$ ) and circles ( $g_L \geq 1.5$ ). There is a clear impact of stellar activity on the EW of Fe I, and it tends to increase with  $\log_{10}(\tau_{\lambda})$  (upper panel of Fig. 2). The Fe I lines with smaller  $\tau_{\lambda}$ , meaning those closer to the base of the chromosphere, are the most affected, as they have the largest variations in  $\Delta\text{EW}$  (Fig. 2). We also find a clear correlation between  $\Delta\text{EW}$  and  $g_L$  for  $\text{EW} > 40$  mÅ at fixed  $\tau_{\lambda}$ ; however we do not found correlations with another parameters as wavelength, excitation potential and  $\log g f$ . The bottom panel of Fig. 2 shows that 3 Fe II lines are sensitive to stellar activity, and we could infer a similar behavior as the Fe I lines. In panel (b) of Fig. 1 is shown the relative variations of EWs of Fe I lines along the stellar activity cycle. A similar modulation is found for Fe II but with lower amplitude. We also detected EW variations of iron lines found in the literature (see Table 1).

### 3.3 Stellar Parameters

We determined the iron abundances (adopting lines only from Meléndez et al. (2014)) using the MOOG code and the Kurucz ODFNEW model atmospheres (Castelli & Kurucz 2003). The stellar parameters along the stellar cycle (i.e., for each bin in panel (b) in Fig. 1) were estimated through the spectroscopic equilibrium using the *qoyllur-quipu* ( $q^2$ ) code (see Table 2). The method was purely differential between the Sun and HIP 36515.

Panel (a) of Fig. 3 shows a fairly strong Spearman anti-correlation ( $-0.94$ ,  $p\text{-value}=0.005$ ) between  $T_{\text{eff}}$  and  $S_{\text{HK}}$ . The maximum change observed in  $T_{\text{eff}}$  is 27 K, which is significant considering our high precision of 15 K. From our line list of 104 iron lines, we find that 46 are affected by stellar activity (see Table 1). These variations impact the iron abundance determinations (maximum variation of 0.016 dex), resulting in an anti-correlation ( $-0.77$ ,  $p\text{-value}=0.07$ ) with  $S_{\text{HK}}$  (see panel (b) of Fig. 3). As seen in panel

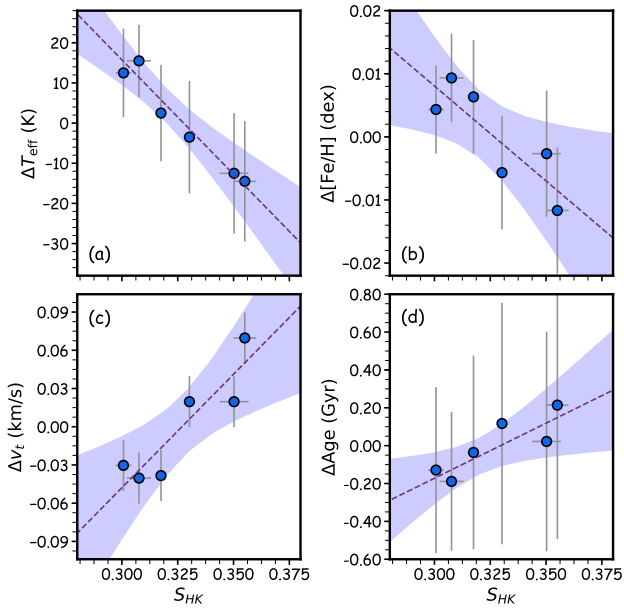


**Figure 3.** Activity induced variations in  $T_{\text{eff}}$ ,  $[\text{Fe}/\text{H}]$ ,  $v_t$  and age. The dashed lines are the best linear fit to the data points, and have been performed using the Kaptein `kmpfit` package (Terlouw & Vogelaar 2015). Shadows regions represent the 95% confidence interval of the linear fit. The standard deviation of the linear fit for the  $T_{\text{eff}}$ ,  $[\text{Fe}/\text{H}]$ ,  $v_t$ , and age are 3 K, 0.004 dex, 0.02  $\text{km s}^{-1}$  and 0.07 Gyr, respectively.

**Table 1.** Iron line list that are sensitive to stellar activity. <sup>(a)</sup> Shchukina & Trujillo Bueno (2015), <sup>(b)</sup> Fabbian et al. (2012), <sup>(c)</sup> Borrero (2008). This table is available in its entirety in machine readable format at the CDS.

Wavelength (Å)	$\chi_{\text{exc}}$ (eV)	$g_L$ ...	$\log_{10}(\tau_\lambda)$ ...	$\Delta EW$ (mÅ)	$\langle EW \rangle$ (mÅ)
4088.560 <sup>a</sup>	3.640	1.00	-1.16	1.3	54.5
4091.560 <sup>a</sup>	2.830	2.00	-1.39	1.9	59.00
4389.245	0.052	1.50	-2.29	2.1	71.33
4485.970 <sup>a</sup>	3.640	2.75	-0.19	1.0	19.50
4508.288	2.855	0.50	-2.05	1.6	89.85

(c) of Fig. 3,  $v_t$  shows a strong correlation (+0.94, p-value=0.005) with  $S_{\text{HK}}$ . The increase of  $v_t$  with stellar activity could explain the low  $[\text{Fe}/\text{H}]$  observed in star forming regions (Spina et al. 2017); it could be a consequence of changes in the curve of growth due to variations in  $EW$ s of iron lines.

The ages, masses, and radii were estimated using the  $q^2$  code through the grid of Yonsei-Yale isochrones (Yi et al. 2001). The panel (d) of Fig. 3 shows no significant changes in the age determination with the activity cycle, since they agree within their uncertainties. Similar results are found for the mass, radius and  $\log g$  (Table 2).

### 3.4 Lithium abundance

The Li I line at 6707.8 Å is an age indicator in solar twins (Carlos et al. 2016; ?), where younger solar twins are expected to have much larger Li abundances. We analyzed this line along the activity cycle, with the different stellar parameters obtained for each cycle and got very consistent Li abundances. To find the abundances, we fitted synthetic spectra generated with the MOOG code to the observed

spectra, and with  $\chi^2$  minimization found the LTE abundances of  $A(\text{Li}) = 2.65$  dex and  $A(\text{Li}) = 2.66$  dex for the minimum, and maximum of the activity cycle, respectively. A variation of 0.01 dex is within the expected error of our analysis ( $\sigma A(\text{Li}) = 0.03$  dex) and as such we do not consider this to be indicative of any abundance variation within the activity cycle.

In order to detect variations in the Li line, we estimated the  $EW$  of the synthetic line of the best abundance. We measured the synthetic line, instead of directly measuring the observed spectra, due to blends in the Li line (see Fig. 2 of Carlos et al. 2016). Once we found the best Li abundance via synthetic spectra fitting, which accounts for all the blends, we can remove all lines, except the Li lines, and create a clear synthetic lithium profile. We measured the  $EW$ s of the synthetic lines using the integrated flux along the Li line profile and found a variation of 4.7 mÅ between the maximum and minimum of the activity cycle (see panel (d) of Fig. 1). The standard deviation is 2.25 mÅ for each measurement. We also estimate the non-LTE abundance via  $EW$  employing the grid of abundances from ? and found non-LTE abundances variations of only 0.01 dex along the activity cycle, fully compatible with the spectral synthesis analysis. Similar results were obtained when the  $EW$ s were measured directly on the observed spectrum using the *splot* task in IRAF. Thus, our analysis show that although there may be minor variations in  $EW$ s, they are likely compensated by the changes in  $T_{\text{eff}}$ , so that there are no significant variations on the abundances of Li during the activity cycle, and any minor variations are likely due to measurement errors.

## 4 CONCLUSIONS

We have performed, for the first time, a high-precision differential abundance analysis of the young solar twin HIP 35615, along different phases of its activity cycle. We used high-quality HARPS spectra in order to quantify the possible impact of stellar activity on the stellar parameters determination and Li abundance. We determined the activity cycle period (~6 years) via Gaussian process fitting. Our iron line list has minimal blending and spans a wide range in oscillator strength, Landé factor, wavelength, and the formation height covers a large region of the photosphere (Fig. 2).

We measured the  $EW$  of the iron lines in six points of the activity cycle. We report for the first time variations of the  $EW$  of several iron lines (43 lines of Fe I and 3 of Fe II) with the stellar activity cycle. These could be used as a new activity indicator for young stars. Despite that these changes are correlated with the Landé factor at fixed  $\tau_\lambda$ , the strongest correlation found is with the height of formation of the iron lines (see Fig. 2), which could indicate a purely chromospheric effect (i.e. chromospheric heating) over the strong iron lines ( $EW > 40$  mÅ). This result makes difficult to conclude if these changes are due to the direct or indirect effects.

We also observe that stellar activity influences the stellar parameters determinations based on spectroscopic equilibrium. The  $EW$  of iron is enhanced during the maximum of the activity cycle, but the impact of activity on the other stellar parameters, results in a decrease of the metallicity. The microturbulence velocity increase with the activity cycle as a consequence of changes in the line profile of iron lines. It is not possible to detect modulations of the surface gravity due to the uncertainties (~0.027 dex). Other fundamental parameters such as age, mass and radius remain almost invariant within measurement uncertainties.

We created a new line list where the iron lines are slightly sensitive to magnetic fields (Table 3). Using this list, we determined



**Table 2.** Stellar and fundamental parameters of HIP 36515 determined in three epochs of the activity cycle. The symbols <sup>(\*)</sup> and <sup>(+)</sup> represent the stellar parameters obtained using the sensitive and non-sensitive iron lines<sup>a</sup> (shown in the shadowed region), respectively.

Cycle ...	$S_{\text{HK}}$ ...	$T_{\text{eff}}$ (K)	$\log g$ (dex)	[Fe/H] (dex)	$v_t$ ( $\text{km s}^{-1}$ )	Age (Gyr)	Mass $M_{\odot}$	Radius $R_{\odot}$
maximum*	$0.355 \pm 0.005$	$5837 \pm 15$	$4.54 \pm 0.027$	$-0.045 \pm 0.010$	$1.30 \pm 0.02$	$0.96 \pm 0.70$	$1.033 \pm 0.009$	$0.941 \pm 0.012$
intermediate*	$0.330 \pm 0.002$	$5848 \pm 14$	$4.53 \pm 0.023$	$-0.039 \pm 0.009$	$1.25 \pm 0.02$	$0.86 \pm 0.64$	$1.038 \pm 0.009$	$0.943 \pm 0.012$
minimum*	$0.301 \pm 0.004$	$5864 \pm 11$	$4.54 \pm 0.020$	$-0.029 \pm 0.007$	$1.19 \pm 0.02$	$0.62 \pm 0.44$	$1.047 \pm 0.005$	$0.945 \pm 0.008$
maximum <sup>+</sup>	$0.355 \pm 0.005$	$5843 \pm 9$	$4.52 \pm 0.015$	$-0.024 \pm 0.007$	$1.14 \pm 0.03$	$0.65 \pm 0.43$	$1.045 \pm 0.006$	$0.945 \pm 0.007$
intermediate <sup>+</sup>	$0.330 \pm 0.002$	$5838 \pm 8$	$4.51 \pm 0.015$	$-0.030 \pm 0.006$	$1.13 \pm 0.03$	$0.90 \pm 0.63$	$1.039 \pm 0.009$	$0.945 \pm 0.010$
minimum <sup>+</sup>	$0.301 \pm 0.004$	$5843 \pm 9$	$4.52 \pm 0.015$	$-0.032 \pm 0.007$	$1.14 \pm 0.03$	$0.70 \pm 0.48$	$1.041 \pm 0.007$	$0.943 \pm 0.008$

<sup>a</sup> Notice that the list of non-sensitive lines has only two lines at low excitation potential, therefore we suggest caution if this line list is used.

**Table 3.** Iron line list that is non-sensitive to stellar activity. This table is available in its entirety in machine readable format at the CDS.

Wavelength (Å)	Species ...	$\chi_{\text{exc}}$ (eV)	$\log gf$ ...
4365.896	26.0	2.990	-2.250
4445.471	26.0	0.087	-5.441
4523.400	26.0	3.650	-1.960
4556.925	26.0	3.250	-2.660
4576.340	26.1	2.844	-2.950

the stellar parameters in each epoch of the cycle, and we recover similar values obtained in the minimum of the activity cycle, except for the  $T_{\text{eff}}$  (see the shadowed region in Table 2). It is possible that these values found represent the true stellar parameters of HIP 36515. If spectroscopic observations are available at several phases of the activity cycle, we recommend adopting the stellar parameters determined at the minimum of the activity cycle.

The  $EW$  of the Li I line at 6707.8 Å was measured along the activity cycle, and we found a minor variation of the  $EW$ s (panel (c) of Fig. 1). However, we found almost no variations of their abundance because the  $EW$ s are compensated with the  $T_{\text{eff}}$  estimated for each epoch of the activity cycle.

This experiment, made with a solar twin of 0.4 Gyr, should be repeated with even younger solar twins, as the effects could be much stronger, specially for Sun-like stars with ages <250 Myr, where the magnetic field strength is significantly higher (Rosén et al. 2016).

## ACKNOWLEDGMENTS

J.Y.G. acknowledges the support from CNPq. D.L.O. and J.M. thank the support from FAPESP (2016/20667-8; 2018/04055-8). L.S. acknowledge financial support from the Australian Research Council (Discovery Project 170100521). This work was performed under contract with the California Institute of Technology (Caltech)/Jet Propulsion Laboratory (JPL) funded by NASA through the Sagan Fellowship Program executed by the NASA Exoplanet Science Institute (R.D.H.).

## REFERENCES

Ambikasaran S., Foreman-Mackey D., Greengard L., Hogg D. W., O’Neil M., 2015, *IEEE Transactions on Pattern Analysis and Machine Intelligence*, 38  
 Barrado y Navascues D., Fernandez-Figueroa M. J., Garcia Lopez R. J., de Castro E., Cornide M., 1997, *A&A*, 326, 780

Bedell M., Meléndez J., Bean J. L., Ramírez I., Leite P., Asplund M., 2014, *ApJ*, 795, 23  
 Borrero J. M., 2008, *ApJ*, 673, 470  
 Campante T. L., et al., 2014, *ApJ*, 783, 123  
 Carlos M., Nissen P. E., Meléndez J., 2016, *A&A*, 587, A100  
 Casagrande L., Ramírez I., Meléndez J., Bessell M., Asplund M., 2010, *A&A*, 512, A54  
 Castelli F., Kurucz R. L., 2003, in Piskunov N., Weiss W. W., Gray D. F., eds, *IAU Symposium Vol. 210, Modelling of Stellar Atmospheres*. p. A20 ([arXiv:astro-ph/0405087](https://arxiv.org/abs/astro-ph/0405087))  
 Do Nascimento Jr. J. D., Castro M., Meléndez J., Bazot M., Théado S., Porto de Mello G. F., de Medeiros J. R., 2009, *A&A*, 501, 687  
 Edmonds F. N. J., 1969, *J. Quant. Spectrosc. Radiative Transfer*, 9, 1427  
 Fabbian D., Khomenko E., Moreno-Inertis F., Nordlund Å., 2010, *ApJ*, 724, 1536  
 Fabbian D., Moreno-Inertis F., Khomenko E., Nordlund Å., 2012, *A&A*, 548, A35  
 Fekel F. C., 1996, in Strassmeier K. G., Linsky J. L., eds, *IAU Symposium Vol. 176, Stellar Surface Structure*. p. 345  
 Flores M., González J. F., Jaque Arancibia M., Buccino A., Saffé C., 2016, *A&A*, 589, A135  
 Flores M., González J. F., Jaque Arancibia M., Saffé C., Buccino A., López F. M., Ibañez Bustos R. V., Miquelarena P., 2018, *A&A*, 620, A34  
 Ghezzi L., Cunha K., Smith V. V., de la Reza R., 2010, *ApJ*, 724, 154  
 Giampapa M. S., 1984, *ApJ*, 277, 235  
 Gustafsson B., Edvardsson B., Eriksson K., Jørgensen U. G., Nordlund Å., Plez B., 2008, *A&A*, 486, 951  
 Hekker S., Elsworth Y., Mosser B., Kallinger T., Basu S., Chaplin W. J., Stello D., 2013, *A&A*, 556, A59  
 Livingston W., Wallace L., White O. R., Giampapa M. S., 2007, *ApJ*, 657, 1137  
 Lorenzo-Oliveira D., et al., 2018, *A&A*, 619, A73  
 Lorenzo-Oliveira D., et al., 2019, *MNRAS*, 485, L68  
 Meléndez J., Dodds-Eden K., Robles J. A., 2006, *ApJ*, 641, L133  
 Meléndez J., Asplund M., Gustafsson B., Yong D., 2009, *ApJ*, 704, L66  
 Meléndez J., et al., 2014, *ApJ*, 791, 14  
 Montes D., Ramsey L. W., 1998, *A&A*, 340, L5  
 Moore C. S., Uitenbroek H., Rempel M., Criscuolo S., Rast M. P., 2015, *ApJ*, 799, 150  
 Pallavicini R., Randich S., Giampapa M. S., 1992, *A&A*, 253, 185  
 Ramírez I., et al., 2014, *A&A*, 572, A48  
 Rasmussen C. E., Williams C. K. I., 2006, *Gaussian Processes for Machine Learning*  
 Rosén L., Kochukhov O., Hackman T., Lehtinen J., 2016, *A&A*, 593, A35  
 Schuler S. C., King J. R., Terndrup D. M., Pinsonneault M. H., Murray N., Hobbs L. M., 2006, *ApJ*, 636, 432  
 Shchukina N., Trujillo Bueno J., 2015, *A&A*, 579, A112  
 Shchukina N., Sukhorukov A., Trujillo Bueno J., 2016, *A&A*, 586, A145  
 Sneden C. A., 1973, PhD thesis, THE UNIVERSITY OF TEXAS AT AUSTIN.  
 Spina L., et al., 2014, *A&A*, 567, A55  
 Spina L., et al., 2017, *A&A*, 601, A70  
 Spina L., et al., 2018, *MNRAS*, 474, 2580

- Steenbock W., Holweger H., 1981, *A&A*, **99**, 192
- Terlouw J. P., Vogelaar M. G. R., 2015, Kapteyn Package, version 2.3.  
Kapteyn Astronomical Institute, Groningen
- Yana Galarza J., Meléndez J., Ramírez I., Yong D., Karakas A. I., Asplund M., Liu F., 2016, *A&A*, **589**, A17
- Yi S., Demarque P., Kim Y.-C., Lee Y.-W., Ree C. H., Lejeune T., Barnes S., 2001, *ApJS*, **136**, 417

This paper has been typeset from a  $\text{\LaTeX}$  file prepared by the author.